MuB is an AAA+ ATPase that forms helical filaments to control target selection for DNA transposition

Naoko Mizuno[a,b], Marija Dramićanin[c], Michiyo Mizuuchi[d], Julia Adam[b], Yi Wang[d,e], Yong-Woon Han[d,f], Wei Yang[d], Alasdair C. Steven[a], Kiyoshi Mizuuchi[d,1], and Santiago Ramón-Maiques[c,d,1]

[a]Laboratory of Structural Biology, National Institute of Arthritis, Musculoskeletal, and Skin Diseases and [d]Laboratory of Molecular Biology, National Institute of Diabetes and Digestive and Kidney Diseases, National Institutes of Health, Bethesda, MD 20892; [b]Max Planck Institute of Biochemistry, D-82152 Martinsried, Germany; [c]Structural Bases of Genome Integrity Group, Structural Biology and Biocomputing Programme, Spanish National Cancer Research Centre (CNIO), 28029 Madrid, Spain; [e]Department of Biochemistry and Molecular Biology, Baylor College of Medicine, Houston, TX 77030; and [f]Institute for Integrated Cell-Material Science, Kyoto University, Kyoto 606-8501, Japan

Contributed by Kiyoshi Mizuuchi, May 20, 2013 (sent for review March 29, 2013)

MuB is an ATP-dependent nonspecific DNA-binding protein that regulates the activity of the MuA transposase and captures target DNA for transposition. Mechanistic understanding of MuB function has previously been hindered by MuB's poor solubility. Here we combine bioinformatic, mutagenic, biochemical, and electron microscopic analyses to unmask the structure and function of MuB. We demonstrate that MuB is an ATPase associated with diverse cellular activities (AAA+ ATPase) and forms ATP-dependent filaments with or without DNA. We also identify critical residues for MuB's ATPase, DNA binding, protein polymerization, and MuA interaction activities. Using single-particle electron microscopy, we show that MuB assembles into a helical filament, which binds the DNA in the axial channel. The helical parameters of the MuB filament do not match those of the coated DNA. Despite this protein–DNA symmetry mismatch, MuB does not deform the DNA duplex. These findings, together with the influence of MuB filament size on strand-transfer efficiency, lead to a model in which MuB-imposed symmetry transiently deforms the DNA at the boundary of the MuB filament and results in a bent DNA favored by MuA for transposition.

Phage Mu | nucleoprotein filament

DNA transposons are ubiquitous in the genomes of all forms of life and play important evolutionary roles in generating gene diversity and in shaping genomic landscapes (1). Although typically transposons exhibit no strong sequence selectivity for the target DNA site, certain transposons avoid self-destructive insertion (reviewed in ref. 2), a phenomenon called "target immunity" because the presence of a copy of the transposon renders nearby DNA sites "immune" to additional insertion by the same transposon (3–8). MuB plays critical roles in this self-immunity in the bacteriophage Mu transposition process.

Phage Mu is one of the most complex and efficient transposable elements (reviewed in refs. 3 and 4). Two phage-coded proteins, MuA and MuB, are essential for efficient Mu transposition. MuA is the transposase responsible for synapsing the two Mu end sequences and for all of the DNA cutting and joining steps in the initial stages of transposition. However, transposition is inefficient in the absence of MuB, and the residual Mu insertion that takes place uses only DNA target sites near or within the transposing element, often leading to self-destruction (9–11). MuB is a small (35-kDa) ATP-dependent nonspecific DNA-binding protein with relatively low ATPase activity (10, 12, 13). Upon ATP binding, MuB polymerizes preferentially on DNA, but in the absence of DNA it still can form polymers of variable sizes (14, 15). When observed by total internal reflection fluorescence microscopy, GFP-MuB-ATP binds along the DNA molecule forming many short separate segments of polymers, and, as more GFP-MuB is added, the protein-covered segments elongate to form an apparently continuous polymer that fully coats the DNA. Hydrolysis of ATP reverses this process, triggering disassembly of the MuB polymer (16–18).

The MuB–DNA complex controls MuA activity at several steps, including stimulation of the strand-transfer reaction, which joins Mu DNA ends to the target DNA site (19, 20), leading to utilization of MuB-bound DNA as the preferred target for transposition (11). MuB-stimulated transposition displays target immunity, avoiding target sites near preexisting Mu-end sequences where MuA binds. This is because MuA stimulates the ATPase activity of MuB, and because this interaction takes place more frequently when the two proteins are bound on the same DNA molecule relatively close to each other, MuA triggers the dissociation of MuB from DNA sites near the Mu ends more efficiently than from those sites at a distance (21). Thus, by the time MuA assembles the active complex with synapsed Mu DNA ends ready to capture target DNA, MuB has been depleted from the vicinity of the active complex and accumulates on DNA sites away from the Mu-end sequence. This explains the strong preference of the transposing Mu to target DNA sites at substantial distances away (5–25 kb) from its original site (22).

Beyond the mechanistic framework outlined above, study of MuB function has been hampered by the lack of structural information. The 312-amino-acid MuB polypeptide can be divided into two fragments by limited proteolysis (23). The N-terminal 25-kDa fragment contains Walker A and Walker B motifs (24) and also a putative helix-turn-helix motif (12), but it lacks ATPase activity and is prone to aggregate. The C-terminal 10-kDa fragment consists of a four-helix bundle, whose structure was de-

Significance

DNA transposons move from one genomic location to another using a transposase. A regulatory protein might assist in target selection and avoiding self-destruction. MuB is the regulatory protein of Mu transposon. Here we report that MuB is an AAA+ (ATPase associated with diverse cellular activities) ATPase and forms right-handed helical filaments around DNA. The helical parameters of MuB and DNA are mismatched and their interactions are nonuniform. We propose that enhanced ATP hydrolysis by MuB, induced by contacts with the MuA-transposon-end complex, leads to DNA deformation and bending at the MuB filament end, thus creating a favored target for transposition.

Author contributions: N.M., W.Y., A.C.S., K.M., and S.R.-M. designed research; N.M., M.D., M.M., J.A., Y.W., Y.-W.H., K.M., and S.R.-M. performed research; N.M., M.D., M.M., J.A., Y.W., Y.-W.H., W.Y., A.C.S., K.M., and S.R.-M. analyzed data; and N.M., W.Y., A.C.S., K.M., and S.R.-M. wrote the paper.

The authors declare no conflict of interest.

Data Deposition: The cryo-EM maps of the MuBwt DNA(–), MuBwt DNA(+) and MuB-ΔN DNA(+) filaments have been deposited in the Electron Microscopy Data Bank under the accession codes EMDB-2395, EMDB-2398, and EMDB-2400, respectively.

[1]To whom correspondence may be addressed. E-mail: sramon@cnio.es or kiyoshimi@helix.nih.gov.

This article contains supporting information online at www.pnas.org/lookup/suppl/doi:10.1073/pnas.1309499110/-/DCSupplemental.

termined by NMR spectroscopy and reported to resemble the N-terminal domain of *Escherichia coli* replicative helicase DnaB (25) (Fig. S1). Beyond this, no sequence similarity between MuB and other proteins has been reported. Studies of mutant proteins have been limited mostly to those involving the Walker motifs (26). MuB's tendency to aggregate in the presence of ATP hampered efforts at structural characterization. Without such information, it has not been clear how ATP controls MuB polymerization, what kind of polymer MuB forms, how MuB polymer interacts with DNA, or how MuA interacts with MuB polymer and triggers ATP hydrolysis and DNA dissociation.

In this study we combine bioinformatic, mutagenic, biochemical, and electron microscopy (EM) techniques to characterize the structure of MuB and its role in DNA binding and transposition. First, we present evidence that MuB is a member of the AAA+ (*A*TPases *A*ssociated with diverse cellular *A*ctivities) ATPase superfamily. A large number of these proteins have been studied structurally and functionally (27, 28). Guided by this finding, we identified the critical residues that control MuB ATPase, DNA substrate binding, and protein polymerization, yielding a clear picture of the communication between MuB and its interaction partners, MuA and DNA. Furthermore, we studied the structure of MuB polymers by cryo-EM and image reconstruction. We demonstrate that MuB-ATP forms a solenoid-like filament (150 Å in diameter with a pitch of 48 Å) and that DNA is bound in the axial channel. The helical parameters of the MuB filament (5.4 subunits and 48-Å per turn) do not match those of the B-form DNA (10 bp and 36 Å per turn). However, despite this mismatched symmetry between the protein and DNA, MuB does not significantly distort the bound DNA duplex. Therefore, individual MuB subunits in the filament must interact with DNA nonuniformly.

Results

MuB Is Predicted to Be an AAA+ ATPase. We used the protein structure prediction servers PHYRE (29) and HHpred (30) to search for structural homologs of MuB. Notably, all of the proteins identified as having high similarity to MuB are members of the AAA+ ATPase superfamily. Despite the rather limited sequence identities (8–17%), all of the alignments predicted MuB residues 77–312 to have the same secondary and tertiary structures as the AAA+ proteins (Fig. 1*A*). Proteolytic cleavage was observed between I231 and N232 that separates the two putative domains of the AAA+ module in MuB (Fig. 1 *A* and *B*; Fig. S2*A*).

To test the MuB functional organization, we engineered a construct consisting only of the putative AAA+ module (MuB-ΔN; residues 65–312) and another construct lacking the C-terminal domain (MuB-ΔC; residues 1–231). Whereas MuB-ΔC lacks any ATPase activity and has low expression and low solubility, MuB-ΔN is soluble and stable and exhibits the ATPase activity at 50% of full-length MuB (k_{obs} = 3.2 min^{-1}) (Fig. 2*A*). It is known that ATP hydrolysis is inhibited by DNA and is significantly stimulated by MuA in the presence of DNA (but not by a truncated form of MuA lacking the C-terminal 48 residues, MuA_{trun}) (10, 14). We observed that the activity of MuB-ΔN responds to the addition of MuA and DNA in a similar manner as wild-type MuB (MuBwt) (Fig. 2 *A*–*C*). Consistently, MuB-ΔN stimulated the intermolecular transposition reaction and discriminated against "immune" target DNA in a cell-free reaction system, similarly to MuBwt (Fig. 2*D*). We also produced two MuB constructs covering residues 1–63 or 1–72, and preliminary characterization indicated that this N-terminal appendage is a well-folded helix-rich globular domain. These results confirm that MuB consists of an AAA+ module preceded by an independently folded N-terminal domain, which can be removed without severely impeding ATP hydrolysis, MuA interaction, or DNA binding.

Identification of AAA+ Sensors, Arginine Finger, and DNA-Binding Loop. In addition to the Walker motifs, AAA+ ATPases possess characteristic residues involved in ATP binding or hydrolysis. In MuB, the importance of the Walker A and Walker B motifs was demonstrated previously: mutations K106A (Walker A) and E174Q or D176H (Walker B) strongly diminished ATPase activity (26). Our similarity analysis predicts that MuB residues N202, R268, and R224 are the sensor I, sensor II, and the arginine finger (R finger), respectively (Fig. 1*A*). Mutations N202A and R224A decreased the ATPase activity ∼60-fold compared with MuBwt, whereas the activity of R268A was practically undetectable (Fig. 2*A*). Two other arginines, R187 and R220, were predicted to be at the same protein interface as the R finger, and mutations of these residues to alanine reduced the ATPase rate by 20- and 12-fold, respectively. The significance of these arginines is discussed below.

To distinguish between defects in ATP hydrolysis versus ATP binding, we measured MuB–ATP/ADP complex formation by a spin-column method (31, 32) (Fig. 2*C*). MuBwt formed a very small amount of nucleotide-bound complex detectable by this method, indicating that ATP dissociation is fast or, more likely, that during the time needed to process the sample (∼1 min) ATP is hydrolyzed (ATPase turnover is $t_{1/2}$ = 19 s) and ADP dissociates. Indeed, the nucleotide-bound fraction increased to ∼60% when DNA was added to the mixture, reflecting ATPase inhibition by DNA. Similarly, 20% of MuB-ΔN eluted from the column bound to the nucleotide, likely due to its reduced ATPase rate, and the nucleotide-bound fraction increased fourfold in the presence of DNA. We expected to detect more nucleotide-bound protein for mutants that bind, but could not hydrolyze ATP with this assay. This was the case for N202A and R187A. In contrast, the nucleotide-bound fraction of R220A, R224A, and R268A was less than 5%, indicating impaired ATP binding. Interestingly, the addition of DNA increased ATP binding especially for mutants with weak ATP binding (Fig. 2*C*), suggesting cooperative stabilization of ATP and DNA binding, leading to MuB polymer formation (see below). Probably due to the improved binding of ATP, addition of DNA enhances the ATPase rates of R187A and R220A (Fig. 2*A*).

A key element that is conserved in a large number of AAA+ proteins is a loop (loop 1) that protrudes from helix α2 and is involved in substrate (protein or DNA) recognition (Fig. 1 *A* and *B*). In MuB, an eight-residue loop is predicted to protrude from the middle of helix α2. We made the triple mutation R150A/R151G/K152A and the double mutation R151A/K152A in this putative loop. These mutants have ATPase activities ∼1.5- and 2-fold higher than MuBwt, but importantly, the activity is unaffected by DNA (Fig. 2*A*). The ATPase activity does not respond significantly to MuA either, indicating that MuB-DNA binding is required for the ATPase to be stimulated by MuA (Fig. 2*B*). We examined the contribution of each of the three residues to the higher activity and/or to the recognition of DNA. R150A, R151A, and K152A single mutants exhibited activities equal, 1.7-, and 2-fold higher than MuBwt, respectively, but, unlike the multiple mutants, the activity was inhibited by the addition of DNA, and K152A was stimulated by MuA (Fig. 2 *A* and *B*). These results indicate that both R151 and K152 are involved in the interaction with DNA. Consistent with the above, the triple mutant failed to stimulate strand-transfer reaction, whereas the K152A mutant did not stimulate strand transfer and discriminate against immune target (Fig. S2*B*).

Visualization of ATP-Induced MuB Filaments by EM. Many AAA+ proteins oligomerize into ring-like or helical assemblies with a central pore that binds the substrate (27) (Fig. 1*B*). Because MuB aggregates in the presence of ATP, we examined these aggregates by EM. Negatively stained specimens containing MuB in the presence of ATP revealed that MuB had polymerized into filaments (Fig. 3*A*). Polymerization was fast, with filaments readily visible on grids prepared only a few seconds after mixing MuB and ATP. The filaments had a uniform width of ∼150 Å and varied in length, typically between 200 and 600 Å, and they exhibited a stain-penetrable axial lumen. Ring-shaped particles with a diameter of

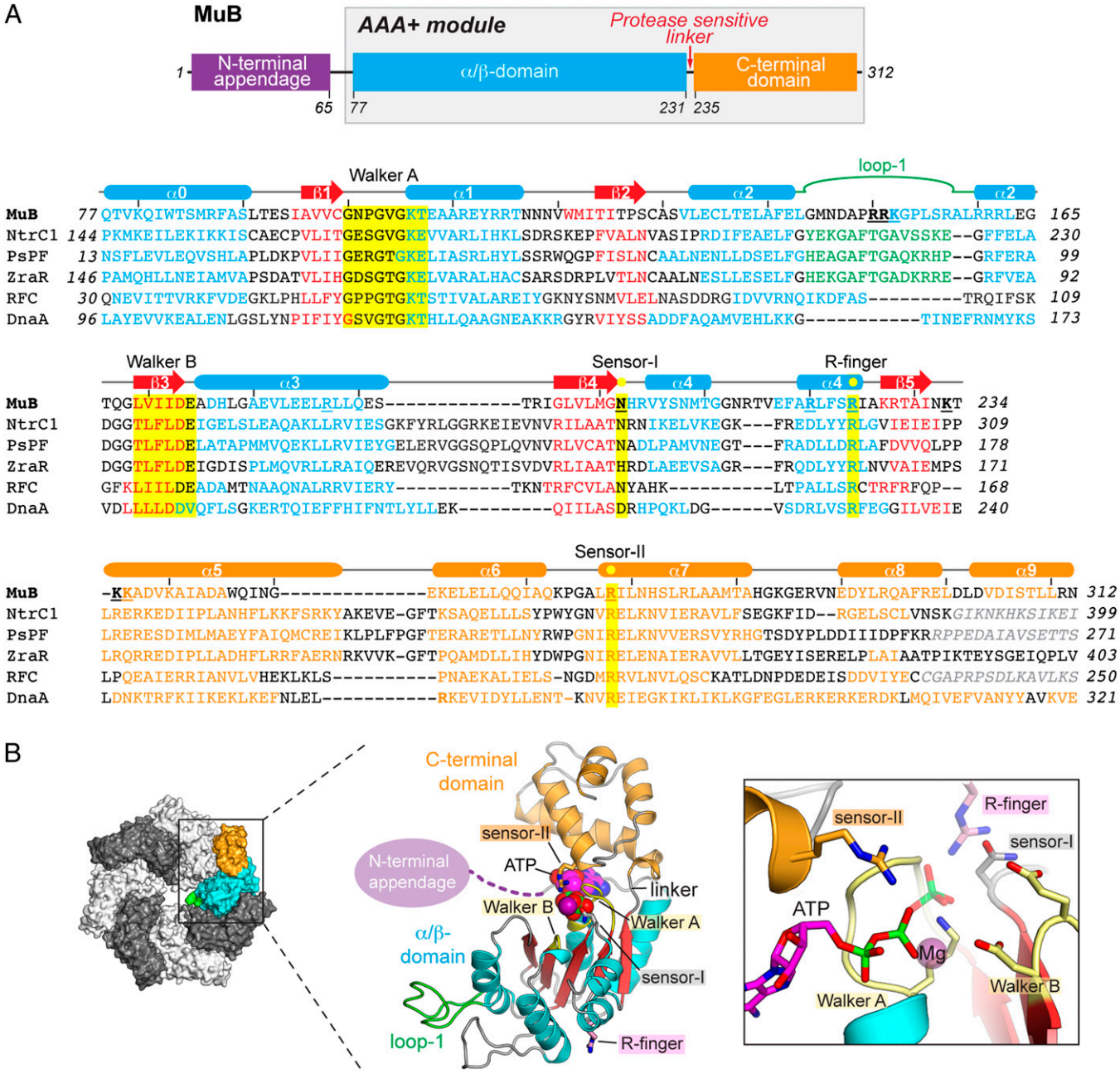

Fig. 1. MuB is an AAA+ ATPase. (*A*) MuB is predicted to have two different segments: (*i*) an N-terminal appendage (in magenta) and (*ii*) an AAA+ module composed of a central α/β-domain (in cyan and red) and a C-terminal helical bundle (in orange). The AAA+ module of MuB is aligned with the AAA+ modules of NtrC1 ([Protein Data Bank (PDB) 1NY5], PsPF [PDB 2BJV], ZraR [PDB 1OJL], RFC [PDB 1SXJ], and DnaA [PDB 3R8F]). Predicted MuB secondary structural elements match those observed in the structures of the aligned proteins. Conserved α-helixes (cylinders) and β-strands (arrows) are represented above the sequences. AAA+ elements are shown with a yellow background. Residues in gray were not observed in the crystal structures. Underscored MuB residues were mutated in this study. (*B*) Representation of the AAA+ fold exemplified by the heptameric ring and subunit structure of NtrC1 bound to ADP (PDB 1NY6). The detailed view of the active site shows the ADP interacting with characteristic AAA+ elements. For illustrative purposes, the ATP γ-phosphate, the Mg^{2+} ion, and the R finger are represented as semitransparent in a simulated position.

150 Å and a hollow center were also seen, which we think represent axial views of short filaments.

Filament formation was not detected without ATP nor with ADP. However, similar filaments were observed in the presence of ATPγS, confirming that ATP binding but not hydrolysis is needed for MuB to polymerize (14). Consistently, the mutant N202A, which can bind but not hydrolyze ATP, forms filaments like those of MuBwt (Fig. S3). On the other hand, with the ATP binding-defective mutants (R268A, R220A, and R224A), polymerization was strongly impaired, and we observed only the ring-shaped particles. One exception was mutant R187A, which despite its capacity to bind ATP did not form regular filaments, suggesting that R187 may contribute to stabilizing the MuB polymerization interface.

MuB-ΔC did not form filaments under any conditions tested. In contrast, MuB-ΔN formed filaments upon ATP addition in a similar manner to MuBwt (Fig. S3), thus proving that the N-terminal appendage is dispensable for this function and that an intact AAA+ module is necessary and sufficient for polymerization.

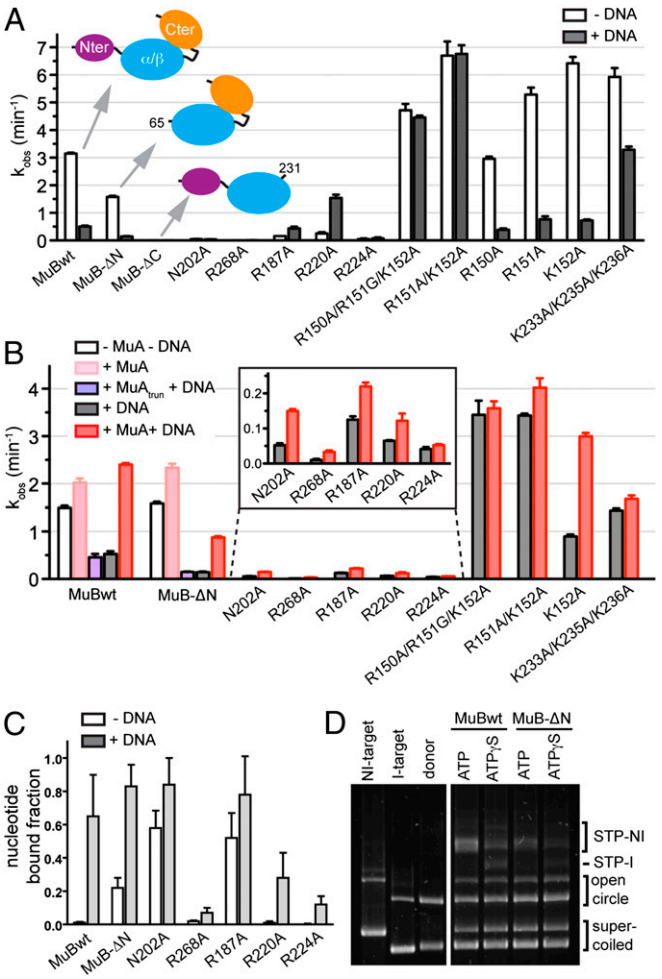

Fig. 2. Site-directed mutagenesis and activity assays confirm the MuB AAA+ elements. (*A*) ATPase activity of MuBwt and mutant forms in the presence and absence of DNA. (*B*) Effect of MuA and DNA on ATPase activity. (*C*) Nucleotide-binding assay by centrifugal gel filtration. (*D*) Strand-transfer stimulation activity of MuBwt and MuB-ΔN. Strand-transfer products (STP) made in reactions that contained both immune (I) and nonimmune (NI) targets and either ATP or ATPγS were examined. Presence of both STP-I and STP-NI in the reaction with ATP, as in reactions in the presence of ATPγS, indicates strand-transfer stimulation without discrimination against immune target. Presence of STP-NI but no (or much less) STP-I in the reaction with ATP indicates strand-transfer stimulation with discrimination against immune target. Also see *SI Materials and Methods* for additional mutants tested.

DNA Stimulates MuB Filament Assembly. ATP-induced MuB filaments are longer in the presence of DNA than without DNA [hereafter named DNA(+) and DNA(−) filaments] (Fig. 3). The median length of the DNA(+) filaments matched the length of the B-form DNA molecules (Fig. 3*D*). Immediately after mixing DNA and MuB in the presence of ATP, short tracts of MuB filament could be seen distributed at irregular intervals along the DNA molecules (Fig. 3*B*, *Inset*), indicating that assembly had initiated at multiple sites. Later in the reaction, fully coated molecules were observed but interrupted with discontinuities, suggesting that the various segments of the MuB filament had met but not annealed (Fig. 3*C*). The filament morphology, other than the length, did not change when DNA was included, suggesting that DNA is inside the filament. In the course of trials, we also found that, by increasing the salt concentration from 0.15 to 0.3 M, MuB-ATP polymerization became DNA-dependent; only long DNA-bound filaments were observed (Fig. 3*C*). This allowed us to specifically prepare DNA(+) MuB filaments.

The N-terminal appendage seems dispensable for DNA interaction because Mu-ΔN polymerizes on DNA as MuBwt does (Fig. S3*A*). On the other hand, mutants with impaired ATP binding (R220A, R224A, and R268A) are also able to polymerize on DNA (Fig. S3*B*), indicating that DNA acts as a scaffold that facilitates ATP binding and protein polymerization. We also observed that the filaments made by the active site mutants responded to MuA stimulation, although the ATPase activity remained low (Fig. 2*B*, *Inset*).

In agreement with the lack of effect by DNA on the ATPase activities of the loop 1 triple and double mutant, the length of the filaments formed by these proteins did not change upon addition of DNA, indicating that they do not bind DNA (Fig. 3*E* and Fig. S3*B*). In contrast, the loop 1 single mutants did assemble into longer filaments on DNA (Fig. S3*B*).

MuB Filaments Are Right-Handed Solenoids with a 48-Å Pitch. Next, MuB-ATP filaments were vitrified and imaged by cryo-EM (Fig. 4). Power spectra of relatively straight filament segments showed a strong layer line, indicative of helical symmetry, at an axial spacing of (48 Å)$^{-1}$ (Fig. S4*A*). Based on the off-meridional positions of these reflections, the layer line was calculated to correspond to a single-start helix; i.e., the filament is a solenoid.

The handedness of the filaments was determined using unidirectionally metal-shadowed specimens (Fig. S4*B*). Filament segments that were optimally oriented relative to the shadowing direction consistently exhibited sets of right-handed striations. This observation was confirmed by the presence of a clear one-sided layer line at (48 Å)$^{-1}$ in averaged power spectra from these images (Fig. S4*B*, *Inset*).

Classification and 3D Reconstruction of MuB Filaments. The images of vitrified MuB filaments were dissected into short segments and subjected to reference-free classification, followed by averaging of the classes thus identified (Fig. 4 and Fig. S5). Comparison between class averages of DNA(+) and DNA(−) filaments did not show clear additional density for the DNA. As discussed below, this is most likely because the DNA density is blurred out upon averaging.

Three-dimensional reconstructions were carried out using the iterative helical real space reconstruction (IHRSR) method (33) (Fig. S5). The reconstructed model shows a solenoid with an axial channel 35–40 Å across; however, discrete subunits were not clearly defined along the solenoid. To refine the analysis, we calculated many reconstructions from subsets of data deemed by the classification procedure to be relatively homogeneous (*Materials and Methods*). These reconstructions all had similar helical symmetries (a 66.2°–67.0° twist and a 8.9- to 9.2-Å rise per asymmetric unit), with ∼5.4 subunits per turn. Some of these reconstructions showed repeating units well (Fig. 5) and were investigated further (see below).

DNA(+) filaments were reconstructed in a similar way. Once again, a global reconstruction yielded poorly defined subunits but classification identified consistent subsets of data whose reconstruction revealed discrete subunits. The reconstruction with the most sharply defined features showed a small density, protruding into the axial channel (Figs. 5 and 6). This may correspond to a DNA-interacting motif of MuB.

In an effort to localize the *N* domain, we recorded images of MuB-ΔN filaments for comparison with filaments of MuBwt (Fig. 4*B* and *SI Materials and Methods*). The reconstructed model of the MuB-ΔN DNA(+) filaments was similar to that of MuBwt. We did not detect discrete density that could be assigned to the *N* domain. The DNA(−) filaments were shorter, and we were unable to perform informative reconstructions of them. The results indicate that the *N* domain is flexibly attached to the AAA+ module. A similar situation has been described for the AAA+ protein unfoldase, ClpA (34, 35).

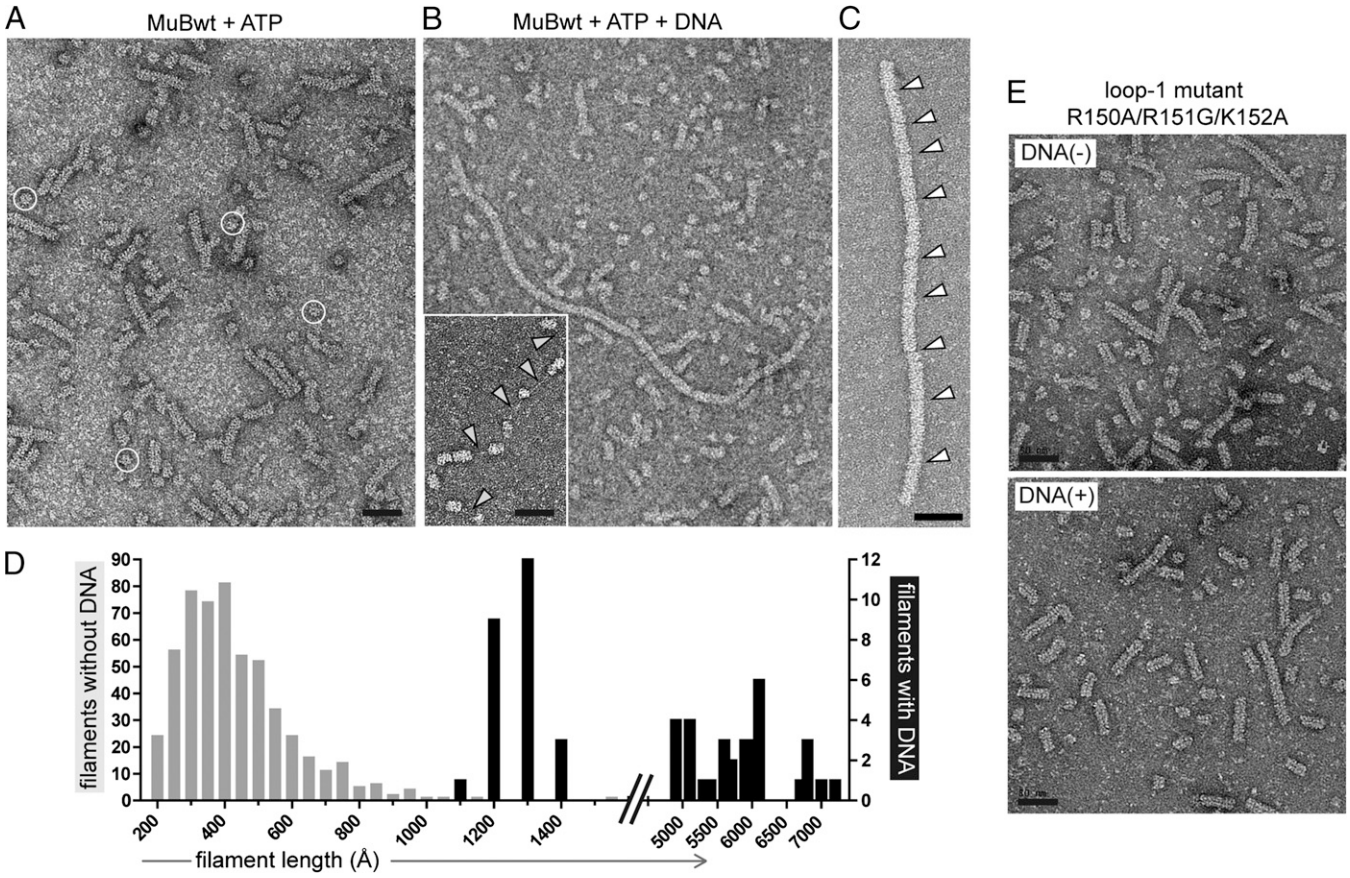

Fig. 3. MuB filaments viewed by negative-staining EM. (*A*) Electron micrograph of negatively stained MuB-ATP filaments. Ring-shaped particles, representing axial views of very short filaments, are encircled. (*B*) MuB filaments assembled in presence DNA. (*Inset*) DNA molecules partially covered by MuB filaments. (*C*) MuB DNA(+) filaments prepared in 300 mM KCl to prevent off-DNA assembly. Arrowheads indicate the discontinuities along the filament. (*D*) Length of DNA(–) (gray; in 150 mM KCl) and DNA(+) filaments (black; in 300 mM KCl). The distribution of the filament lengths agrees with the expected sizes of the DNA fragments: 0.34 kb (~1,200 Å), 1.5 kb (~5,100 Å), 1.7 kb (~5,800 Å), and 1.8 kb (~6,100 Å). (*E*) The filaments of the MuB R150A/R151G/K152A mutant have the same length when adding DNA, indicating that loop 1 is key for DNA recognition. (Scale bars, 500 Å.)

The three reconstructions all have resolutions of about 18 Å (Fig. S5*C*) to which they are limited apparently by disorder. They differ primarily in the near-axial region (Fig. 5). MuBwt DNA(–) has a prominent axial density that we suggest is contributed by *N* domains detached from the wall, at least in this subset of filament segments. This axial density is missing in the other two reconstructions, but on them the density lining the inner surface of the axial channel extends further inward. We suggest that this additional density represents the DNA, although the density is diluted by the randomized averaging process. The *N* domain might be partly contributing to this density, or it could be displaced from an axial location by the DNA to disordered positions outside.

Molecular Docking of an AAA+ Module. The foregoing account assigns the structural units resolved along the strand of the solenoid, mostly if not completely, to the AAA+ module of MuB. We therefore attempted to fit the crystal structure of the AAA+ module of NtrC1 into this density. The numerous crystal structures of different AAA+ modules are sufficiently conserved to suggest that this surrogate should be adequate for docking at the present resolution. We performed a rigid-body fitting to helical units from the reconstructions. The AAA+ module was found to fit quite well into the cryo-EM density (Fig. 6). This modeling experiment implies that the quasi-globular unit of density repeated along the strand consists of the α/β-domain of one subunit and the C-terminal domain of the adjacent subunit. One of the reconstructions of MuBwt with DNA nicely accommodates the density of loop 1 facing the axial channel.

Mutations in the Linker Abolish MuA Stimulation. The proteolytic C-terminal fragment of MuB was previously proposed to bind DNA nonspecifically and to interact with MuA through a patch of three lysines, K233, K235, and K236 (25, 36). We recognized the C-terminal fragment as an integral part of the AAA+ module, which is connected to the α/β-domain by a linker that harbors the three lysines. Because the C-terminal domain and the linker invariably locate at the periphery of the AAA+ assemblies, and in the MuB filament reconstructions they do not face the internal filament channel where DNA binds, we reexamined the role of these lysines in DNA recognition. The MuB K233A/K235A/K236A mutant can polymerize on the DNA and its ATPase activity is inhibited by the addition of DNA (Fig. 2*A* and Fig. S3*B*). Therefore, we concluded that these lysines are not involved in DNA recognition. Interestingly, other AAA+ members (e.g., NtrC1) also present a linker with positively charged residues that undergoes conformational changes associated with the ATPase cycle (37). Thus, an attractive possibility is that the ATPase cycle could be controlled by conformational changes at this linker region. The fact that the triple linker mutant, like the loop 1 mutants, enhances ATPase activity supports this notion (Fig. 2*A*). Because the ATPase activity of the K233A/K235A/K236A mutant and the DNA-bound filaments do not respond to MuA and fail to stimulate strand-transfer

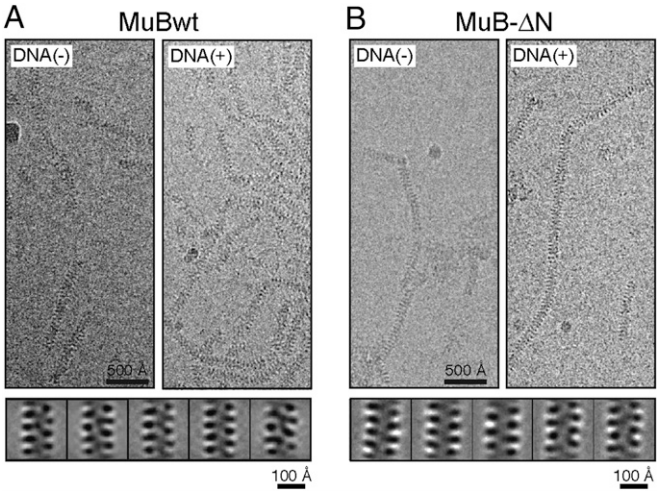

Fig. 4. Cryo-EM images of unstained MuB filaments. (*A*) Images of vitrified MuBwt DNA(–) and DNA(+) filaments and representative class averages obtained from reference-free classification of the DNA(+) filament particles. (*B*) Images of vitrified MuB-ΔN filaments and representative class averages of the DNA(+) filament particles.

reaction (Fig. 2*B* and Fig. S2*B*), these lysine residues most likely interact with MuA to trigger ATP hydrolysis.

MuB Filament Does Not Alter DNA Structure or Topology. The fact that the length of the MuB-DNA filaments matches the length of DNA fragments in the absence of protein (Fig. 3*D*; also see ref. 17) indicates that MuB binding does not significantly alter the DNA length. Next we tested whether the linking number of relaxed circular DNA changes when bound by MuB. Nicked circular pBR322 DNA was converted to a closed circular form in the presence of different concentrations of MuB and ATP, deproteinized, and analyzed by agarose gel electrophoresis in the presence of chloroquine to examine the topoisomer distribution (Fig. S6*A*). The topoisomer distribution broadened in the presence of higher concentrations of MuB, suggesting increased torsional flexibility within the MuB filament. This is unlikely to be caused by increased bending flexibility, considering that the MuB-coated filament appeared stiffer than naked DNA by EM. The center of topoisomer distribution shifted toward reduced linking numbers as more MuB was added to the DNA solution. Combined with the information from the binding titration experiments (see below), we estimate that DNA within MuB-bound filament is only ~1.2% under-wound compared with the relaxed B-form DNA. Therefore, the DNA conformation within the MuB filament appears to be close to the B-form structure.

To measure the MuB saturation density on DNA in solution, we titrated MuB onto fluorescence-labeled DNA and monitored the extent of MuB-DNA association by fluorescence quenching. Based on the titration curve obtained, we estimated that, at the saturation point, each MuB subunit covers ~2.75 bp of the DNA (see details in Fig. S6*B*). This stoichiometry corresponds to 9.3 Å per MuB monomer, which agrees well with the axial rise per MuB monomer in the EM image reconstruction.

Patch Size of MuB-DNA Filament Needed for Transposition Stimulation. The typical size of individual MuB-coated segments along DNA depends on the protein and DNA concentrations and their stoichiometry. To assess the size of the MuB/DNA filament needed to activate the strand-transfer step of transposition, we asked how the MuB concentration or stoichiometry with DNA affects the efficiency of transposition. At MuB concentrations below 10 nM, the target DNA strand-transfer efficiency was sigmoidal in response to the increase of MuB concentration in agreement with the necessity of MuB oligomerization for DNA binding (Fig. S7*A*). At moderately higher MuB concentrations, the reaction efficiency increased roughly linearly with MuB concentration, producing one transposition product per ~50–100 MuB monomers. The higher the density of MuB on DNA, the more efficiently the MuB-bound DNA fragment was used as a target. However, when DNA was completely saturated by bound MuB, it suddenly became a poor strand-transfer target, and only 20% of the DNA was used for transposition (Fig. S7*B*). The inhibition of transposition by saturating MuB concentration was more severe when ATP was substituted by ATPγS (Fig. S7*C*). Thus, a rather large MuB filament on the DNA, perhaps involving several turns or larger, is needed to promote each strand-transfer event, but DNA inside the MuB filament cannot be used as a target, and the actual target site would have to be on the outside of the filament. Thus, either naked DNA adjacent to a MuB filament must be available or the MuA-Mu DNA end complex must generate a MuB-free zone by activating the MuB ATPase activity.

Discussion

Architecture and Domain Functions of the MuB AAA+ ATPase. The AAA+ superfamily is characterized by a two-domain ATPase module that typically oligomerizes into ring-like or helical assemblies. Additional regulatory domains may be added at the N terminus (as in MuB) or at another site. The identification of the AAA+ module of MuB (amino acids 70–312), based on sequence align-

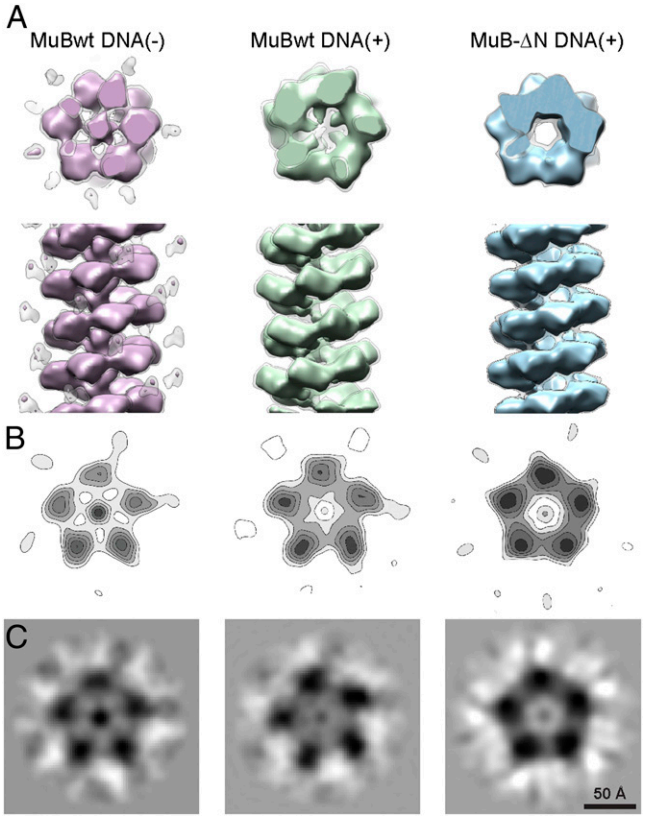

Fig. 5. Three-dimensional reconstructions of MuB filaments. (*A*) Perpendicular views of 3D reconstructions of MuBwt DNA(–) (pink), MuBwt DNA(+) (green), and MuB-ΔN DNA(+) (blue) filaments. The white contour depicts 100% of mass from the calculated molecular weight of the corresponding proteins, whereas the solid-colored densities show the mass calculated from MuB-ΔN. (*B*) Contoured density from one turn of the filament (~48 Å) projected along the filamentous axis. (*C*) Gray scale representation of *B*.

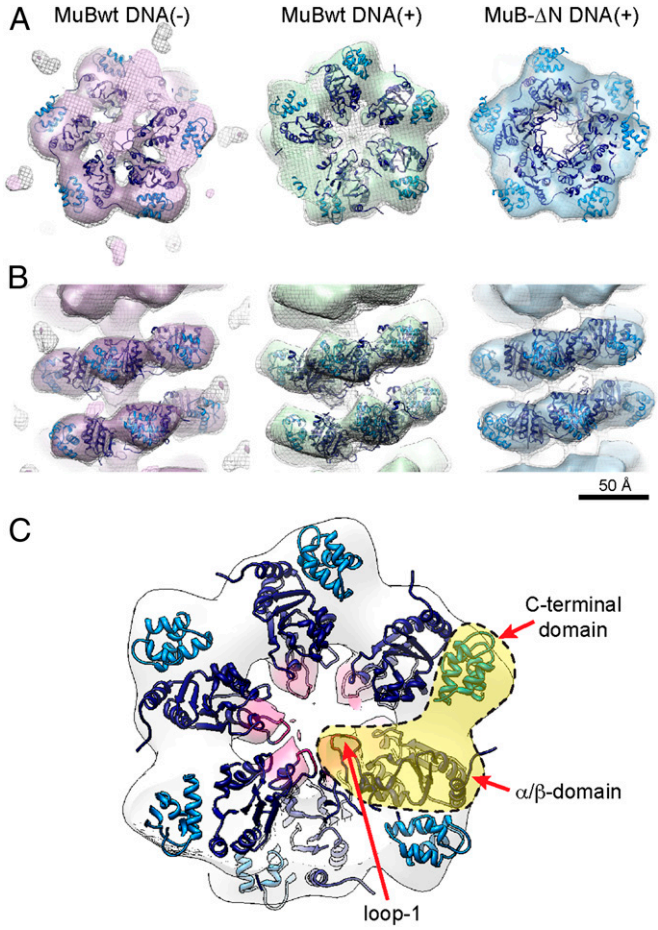

Fig. 6. Molecular docking of an atomic model to MuB envelopes. (*A* and *B*) Perpendicular views of the rigid-body fitting of the NtrC1 AAA+ module into the filament envelops of MuB filaments. (*C*) Detail of the fitting. The densities protruding toward the axial channel could correspond to the DNA binding loop 1.

ment and mutagenesis, led to identification of many functionally important residues. Helical filaments assembled from MuB-ATP, visualized by EM, further support the assignment of MuB as an AAA+ family member. Previously, the division of MuB into two fragments by limited proteolysis led to difficulties in assigning functions to the respective fragments. We demonstrated that the N-terminal ~70 amino acids of MuB constitute an independently folded appendage, loosely attached to the AAA+ ATPase core. This appendage appears to play a relatively minor role in the known biochemical activities of MuB. Further study will be needed to clarify its function.

The 3D structure of the C-terminal domain, which was obtained by denaturation and refolding and determined by NMR under high-salt conditions, clearly differs from the conserved fold of the AAA+ C-terminal domain (reviewed in ref. 38) (Fig. S1). Thus, the C-terminal domain of MuB might fold in a different configuration when isolated on its own, compared with its structure within the context of the intact protein.

Identification of Residues Critical for MuB Filament Formation. We have identified characteristic AAA+ functional elements on MuB: sensor I, sensor II, and R finger. Mutation of these residues strongly affects ATP binding/hydrolysis. Sensor I is typically involved in the coordination of the Mg^{2+} and the attacking water. We assigned N202 to be the sensor I of MuB. As predicted, the mutation N202A strongly impairs ATP hydrolysis, seemingly without affecting ATP binding or filament formation.

Sensor II is typically an arginine whose side chain extends from the C-terminal domain toward the β- and γ-phosphates of ATP, contributing to ATP binding and hydrolysis. We propose that R268 is the sensor II of MuB. When mutated to alanine, ATP binding is impaired and so is the ATPase activity, and no filament formation takes place. The fact that this mutation has the lowest ATPase activity of all of the mutants studied here is intriguing because mutating sensor II in other AAA+ proteins causes only a modest decrease in ATPase activity or has no effect on oligomerization (reviewed in ref. 28). This suggests that the C-terminal domain of MuB might be flexible and that R268 plays a key role in coupling the ATP binding to locking the C-terminal domain in a conformation that favors protein–protein interactions and filament assembly.

The R finger projects from a conserved position on helix α4 and interacts with the γ-phosphate of the ATP bound to the neighboring subunit. Thus, ATP glues adjacent subunits together, favoring and, in some cases, as in MuB, triggering polymerization. In most AAA+ proteins, mutation of the R finger typically impairs ATP hydrolysis and can affect oligomerization. We propose that R224 plays the role of R finger in MuB, and, indeed, the mutation R224A severely impairs ATP binding and filament formation. However, AAA+ members typically have other arginine residues located on the same surface as the R finger that also point toward the active site in the neighboring subunit. We mutated two additional arginines in MuB, which were predicted to be on the same protein surface as the R finger. R220 occupies an equivalent position to an extra arginine in helix α4 of DnaA that projects parallel to the R finger and forms a salt bridge with sensor I in the adjacent subunit. The mutation R220A in MuB impairs ATP binding and filament formation. On the other hand, R187 aligns with an arginine that in RFC directly interacts with the γ-phosphate of ATP. In agreement with this, MuB R187A can bind but not hydrolyze ATP. The R187A mutant is also compromised in filament formation, which in this case cannot be assigned to a defect in nucleotide binding. Thus, we propose that an electrostatic interaction between R187 and the ATP γ-phosphate may contribute to stabilizing this protein interface. Oligomerization of other AAA+ members has been shown to be sensitive to salt concentration, indicating the importance of electrostatic interactions. Likewise, MuB filament formation is salt concentration-sensitive. We propose that these three arginines cooperate in stabilizing the polymerization interface in the presence of ATP. Single-mutant proteins, although compromised, can still form filaments on DNA, which can interact with MuA and activate the target DNA for strand transfer in the presence of ATPγS, albeit very weakly (Fig. S2*B*).

Residues Critical for DNA Binding. Identification of the DNA-binding motif in MuB was guided by sequence alignment with the enhancer-binding proteins NtrC1, PsPF, and ZraR. These proteins have a conserved sequence in loop 1 that is important for interaction with the σ-subunit of RNA polymerase (39). When assembled into rings, loop 1 of each protomer points to the central pore where the σ-subunit binds. Similarly, we hypothesized that the sequence ^{140}PRRKGP^{154}, at the predicted loop 1 in MuB, could face the inner channel and interact with DNA. Results obtained with the double and triple loop 1 mutants support this idea because their ATPase activity is not inhibited by the addition of DNA and the filaments fail to assemble on the DNA. Synergistic effects of two mutations, R151A and K152A, are needed to eliminate DNA recognition because point mutations do not abolish DNA binding.

Interestingly, mutations in loop 1 increase the ATPase approximately twofold. It is known that the addition of DNA lowers the apparent K_d for ATP and slows down ATP hydrolysis. This implies that loop 1 DNA binding allosterically controls the

ATPase active site for tighter ATP binding and slower hydrolysis. The structures of NtrC1, PsPF, and ZraR free or bound to different nucleotides have revealed a nucleotide-dependent movement of loop 1 that might control the interaction with the σ-subunit (37). A similar mechanism in MuB would explain why mutations in loop 1 could uncouple DNA recognition and the ATPase cycle, allowing faster hydrolysis. Stabilization of the ATP-bound state with hydrolysis inhibition by DNA binding would place the DNA-bound MuB ATPase under stringent control of MuA, which would trigger ATP hydrolysis by contacting the MuB-DNA filament from the outside. This also suggests that ATP hydrolysis would return the loop 1 configuration to a low DNA-affinity state and, combined with weakened contacts between monomers due to the loss of the ATP γ-phosphate, could contribute to rapid disassembly of the MuB filament upon MuA interaction.

Symmetry Mismatch in the MuB Nucleoprotein Filament. MuB coats the DNA without significantly altering its B-form structure. Thus, the helical parameters of the MuB filament do not match those of the DNA within the filament (Fig. 7*A* and Fig. S4*C*). This symmetry mismatch is a feature that, to our knowledge, has not been previously observed in other nucleoprotein filaments. Commonly, protein filaments that contain DNA either adopt a helical symmetry close to that of the standard B-form DNA or impose their symmetry on the DNA, inducing deformations. Well-known examples are the RecA family of ATPases, which assemble into helical filaments on DNA and catalyze homologous DNA pairing and strand exchange. Each monomer binds three nucleotides while extending and untwisting the DNA between the triplets, causing an overall stretching of the DNA molecule (40). Another example is the bacterial DnaA protein, an AAA+ member that assembles into right-handed helices and induces the deformation of DNA in a way similar to the RecA mechanism (41). However, not all nucleoprotein filaments induce DNA deformation. RFC is a complex of five different AAA+ subunits that forms right-handed spirals with roughly the same pitch as B-form DNA, without causing

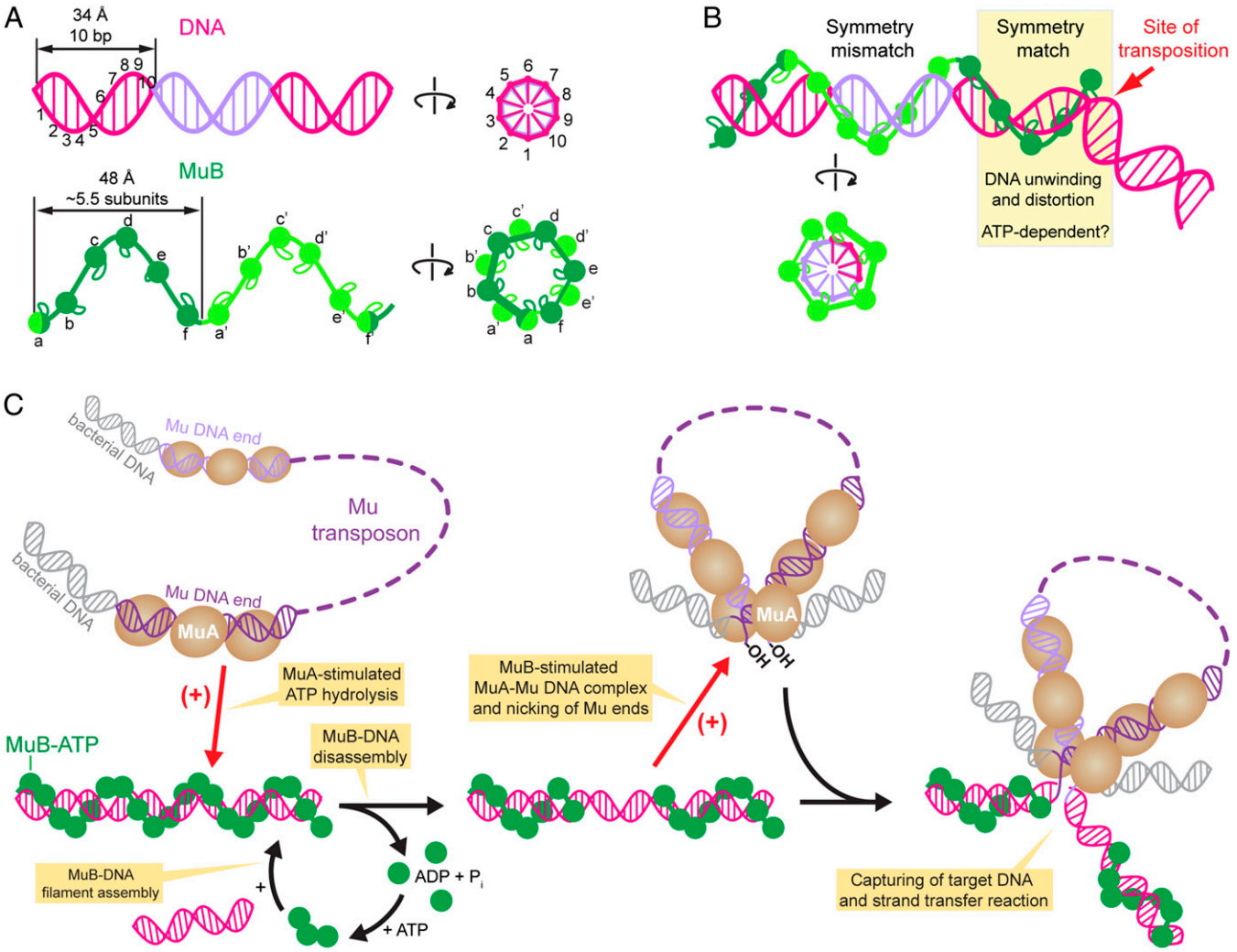

Fig. 7. Model for MuB targeting DNA for transposition. (*A*) The helical parameters of the MuB filament (represented as beads on a string) do not match those of B-form DNA. This results in a nucleoprotein complex with a symmetry mismatch (*B*). Matching symmetry between MuB and DNA would require the DNA to be under-wound and extended, which may occur at the boundary of the MuB filament with the help of MuA and possibly ATP hydrolysis. Deformed and bent DNA is a preferred target for transposition catalyzed by MuA. (*C*) A summary of interplay among MuA, MuB, and DNA during transposition. Upon ATP binding, MuB forms helical filaments on DNA. MuA bound to Mu DNA ends stimulates ATP hydrolysis by MuB and MuB dissociation from DNA, which generates MuB-free DNA regions. Reciprocally, MuB stimulates MuA to pair and nick Mu DNA ends at the junction with the flanking sequences. MuA and MuB together may induce the matching symmetry between MuB and DNA at the boundary of a MuB filament and thus DNA distortion, which leads to the target DNA capture and Mu transposition.

apparent deformations (42). An interesting example is ParA2, a bacterial protein involved in plasmid segregation, which forms left-handed helical filaments on DNA without significantly changing the B-form DNA helicity (43). Unlike RFC, ParA2 filaments do not match the DNA helical parameters, but the arrangement of the helix is dictated by the repetitive interaction of the protein every 8 bp in the DNA, resulting in two different but complementary helices (notably, members of ParA family have been shown to bind DNA distributively as small oligomers, such as MuB, rather than as long filaments when the stoichiometry is low) (44).

The MuB-DNA symmetry mismatch means that the protein–DNA contacts vary from point to point along the filament (Fig. 7*B*). This lack of regularity in MuB-DNA interactions might be a contributing factor for the relatively weak cooperativity in MuB polymerization along DNA, resulting in many short segments of MuB-coated patches at subsaturating MuB concentrations. Weak binding cooperativity would be advantageous so that MuB can be efficiently redistributed by MuA-coupled ATP hydrolysis for transposition immunity.

Another possible consequence of this irregular association with DNA is that not all MuB subunits have loop 1 in the same conformation, and thus the ATPase rate might vary among them. One might ask if the stimulation of MuB ATPase by MuA could be transmitted to the DNA-binding loop, changing its conformation and inducing local changes of the DNA structure. In fact, the most efficient stimulation of MuB ATPase requires a tetramer of MuA molecules bound to the Mu DNA ends, which suggests that multiple nearby MuB monomers might be activated simultaneously. Could this impose local symmetry matching and DNA deformation, which in turn might help utilization of this DNA segment as the strand-transfer substrate for MuA (Fig. 7*B*)? Although MuA lacks sequence specificity, it is known to display a great preference for insertion in mismatch sites on the DNA (45). There is no physiological reason for such preference other than that the mismatch DNA would readily assume a deformed DNA structure, which is favored for the strand-transfer reaction. Indeed, the target DNA segment is severely bent within the structure of the Mu strand-transfer complex (46). Because MuB forms a tightly packed outer shell, the DNA inside the filament would be inaccessible for MuA strand transfer. Indeed, MuB-saturated DNA is a poor target for Mu transposition. Thus, probably, the DNA selected for Mu insertion is not encased within the filament, but it is at the MuB filament boundaries. Then, the hypothetical DNA deformation discussed above perhaps takes place when MuB disassembly is triggered by the MuA–Mu end complex, ready for strand transfer (Fig. 7*C*).

Short helical MuB filaments might be too unstable on DNA and need a minimum of several helical turns to avoid premature dissociation for productive interaction with the MuA-Mu end complex for strand-transfer activation. Perhaps there is an optimal polymer size distribution for function; the MuB architecture described here is well tuned toward this and also to respond efficiently to its interaction with MuA at different stages of the transposition reaction.

What we found in this study has a broader implication for the understanding of the intricate control that AAA+ ATPases could impose in complex reaction systems through their structural components that couple multiple binding partner interactions to the ATPase activity.

Materials and Methods

Proteins. MuB was expressed with N-terminal His-tag cleavable either by thrombin or PreScission protease, and produced essentially as described (18, 26) with two additional steps as detailed in *SI Materials and Methods*. MuA and MuA_{trun} (residues 1–615) were prepared as previously described (47).

Site-Directed Mutagenesis. Mutagenesis was carried out using the QuikChange protocol (Stratagene) by using a pair of mutagenic oligonucleotides and flanking primers, as listed in Table S1, and the amplified fragment with the coding sequence for the mutant protein was inserted into a pOPIN-B vector with In-Fusion. The expression and purification of the mutants was performed as for MuBwt.

ATPase Activity Assays. ATPase assays were carried out as described (18). Reactions contained 1.7 μM MuB (or higher concentrations for the mutants), 25 mM Tris·HCl (pH 8), 0.15 M NaCl, 10 mM $MgCl_2$, 20% (vol/vol) glycerol, 1 mM DTT, 0.1 mg/mL BSA, and 1 mM [α-^{32}P]ATP (4 mCi/μmol). At different time points, 10 μL aliquots were combined with 1.1 μL of 0.5 M EDTA to stop the reaction. Reaction products were separated on polyethyleneimine TLC plates in 0.75 M KH_2PO_4 and quantified using a phosphoimager (Typhoon Trio–GE Healthcare) and ImageQuant software (GE Healthcare). Data were analyzed with Prism 4.0. The inhibitory effect of DNA on the ATPase activity was assayed by adding 1.7 μM of a 36-mer double-stranded DNA. The effects of MuA and MuA_{trun} on the ATPase activity were measured at final protein concentrations of 0.45 μM MuB and 6 μM MuA in the presence of 10 μg/mL pMK589 DNA, which carries a pair of Mu end sequences in wrong orientation (15), and with reaction buffer containing an additional 42 mM KCl.

Nucleotide-Binding Assay. Centrifugal gel filtration (spin-column) assay was carried out essentially as described (31, 32). Fifty-microliter samples of 30 μM MuB in 20 mM Tris·HCl (pH 8), 0.3 M NaCl, 10% (vol/vol) glycerol, and 5 mM $MgCl_2$ were incubated with 1 mM [α-^{32}P]ATP for 0.5 min, applied to tuberculin syringes filled with 1-mL SephadexG-50 (fine) equilibrated in the same buffer, and immediately centrifuged. The unbound nucleotide was retained on the column, and the protein-bound nucleotide in the effluent was quantified using a scintillation counter. Protein recovery in the column effluent was measured by the Bradford method (48). The same DNA used in ATPase activity assays was included at a final concentration of 5 μM to test the effect on nucleotide binding.

Strand-Transfer Immunity Assay. Mu strand-transfer reaction was carried out in two steps. The mini-Mu DNA-MuA complex was assembled in a 25-μL reaction containing 20 μg/mL mini-Mu plasmid DNA (pMK586), 110 nM HU, and 200 nM MuA in 25 mM Hepes (pH 7.6), 1 mM DTT, 100 μg/mL of BSA, 15% (vol/vol) glycerol, 10 mM $MgCl_2$, and 160 mM NaCl at 30 °C for 10 min. The target DNA-MuB complex was assembled in a 12.5-μL reaction containing 30 μg/mL ϕX-RF DNA (nonimmune target), 20 μg/mL pMK589 (immune target containing both Mu end sequences in wrong relative orientation), 500 nM MuA, 500 nM MuB, and 1 mM ATP or ATPγS in the same buffer as above at 30 °C for 30 min. 5-μL of the donor complex and 5-μL of the target complex were combined and incubated for another 20 min. The reaction was stopped by the addition of 20 μg/mL of Proteinase K and incubation at 50 °C for 30 min. The reaction products were analyzed with 0.8% high gelling temperature (HGT) agarose gel electrophoresis.

EM Data Acquisition and Image Processing. For EM specimen preparation, MuB was diluted to 0.07 mg/mL (2 μM) in 30 mM Tris·HCl (pH 8.0), 0.15 M KCl, 5 mM $MgCl_2$, and 1 mM DTT and incubated with 1 mM ATP or ATPγS. After an incubation time between several seconds to 5 min, samples were applied to EM grids. To assemble MuB filaments on DNA, we used a pGEX-6p plasmid with a 1.58-kb fragment inserted between the BamHI and XhoI sites and digested with BamHI, XhoI, AlwNI, and EcoRV (New England Biolabs) to generate four linear DNA fragments of ∼0.3, 1.5, 1.7, and 1.8 kb. Alternatively, gel-purified PCR product of ∼1 kb was used. To selectively obtain MuB filaments on the DNA, the salt concentration in the buffer was increased to 0.3 M. For negative staining, 5 μL of the sample was applied to a glow-discharged carbon-coated copper grid, washed with five drops of dionized water, and stained with two drops of 1% uranyl acetate. The grids were viewed at room temperature with a FEI CM120 electron microscope equipped with a LaB_6 filament and operated at 120 kV. For cryo-EM experiments, 5-μL droplets were applied to Quantifoil holey carbon grids (EMS). A Vitroboot cryo-station (FEI) was used to vitrify the specimen. Imaging was performed with a CM200-FEG electron microscope (FEI) operating at 120 kV. Micrographs were recorded on a 2k × 2k CCD camera (Gatan) with a defocus range of 1.5–3 μm at a nominal magnification of 38,000, corresponding to 2.8 Å per pixel.

Image analysis was carried out using SPIDER (49), EMAN (50), XMIPP (51, 52), and Bsoft (53). The contrast transfer function was corrected by phase-flipping. Filament images were segmented with a box size of 120/80 pixels and 90% overlap of adjacent segments. Totals of 9,717 and 8,342 boxes were selected for MuB in the absence and presence of DNA, respectively, corresponding to ∼36,000 and ∼31,000 asymmetric particles.

For helical parameter determination, the initial helical symmetry was estimated using Fourier transform of MuB filament images. Briefly, a basic layer line (48 Å)$^{-1}$ located at $n = 1$ (basic helix) and then the secondary layer lines at (83 Å)$^{-1}$ were determined to obtain the helical lattice. This layer line was not always fixed at one position, indicative of filament flexibility. IHRSR (33) combined with SPIDER was used for helical symmetrization. The helical parameters were verified by matching the power spectrum of the reprojections of the reconstructions and the averaged power spectrum from raw images.

Reference-free classification, using K-means clustering and principal component analysis, and averaging were performed using EMAN and SPIDER. Individual populations that belong to each class were grouped, and 3D reconstructions for each group were calculated using IHRSR. Reconstructions showing helices with well-defined subunits were further grouped by clustering them according to similar helical parameters, and reconstructions were performed for these classes.

ACKNOWLEDGMENTS. We thank Dr. P. A. Rice for the preliminary sequence-based structural similarity search, which alerted us that MuB belongs to the AAA+ ATPase family; and Dr. U. Baxa for help with the handedness determination. This work was supported by the intramural research programs of the National Institute of Diabetes and Digestive and Kidney Diseases and the National Institute of Arthritis, Musculoskeletal and Skin Diseases of the National Institutes of Health; the Spanish Ministry of Science and Innovation (BFU2010-16812); and Graduiertenkolleg (GRK) 1721 of the Deutsche Forschungsgemeinschaft. M.D. was a recipient of a predoctoral fellowship from the "La Caixa" Foundation. S.R.-M. is a Researcher of the Ramón y Cajal Program of the Spanish Ministry of Economy and Competitiveness.

1. Shapiro JA (2010) Mobile DNA and evolution in the 21st century. *Mob DNA* 1(1):4–18.
2. Craig NL (1997) Target site selection in transposition. *Annu Rev Biochem* 66:437–474.
3. Mizuuchi K (1992) Transpositional recombination: Mechanistic insights from studies of mu and other elements. *Annu Rev Biochem* 61:1011–1051.
4. Chaconas G, Harshey RM (2002) *Mobile DNA II*, eds Craig NL, Craigie R, Gellert M, Lambowitz A (ASM Press, Washington, DC), pp 384–402.
5. Robinson MK, Bennett PM, Richmond MH (1977) Inhibition of TnA translocation by TnA. *J Bacteriol* 129(1):407–414.
6. Lee CH, Bhagwat A, Heffron F (1983) Identification of a transposon Tn3 sequence required for transposition immunity. *Proc Natl Acad Sci USA* 80(22):6765–6769.
7. Hauer B, Shapiro JA (1984) Control of Tn7 transposition. *Mol Gen Genet* 194(1–2): 149–158.
8. Goto N, et al. (1987) Identification of the DNA sequence required for transposition immunity of the gamma delta sequence. *J Bacteriol* 169(9):4388–4390.
9. Craigie R, Arndt-Jovin DJ, Mizuuchi K (1985) A defined system for the DNA strand-transfer reaction at the initiation of bacteriophage Mu transposition: Protein and DNA substrate requirements. *Proc Natl Acad Sci USA* 82(22):7570–7574.
10. Maxwell A, Craigie R, Mizuuchi K (1987) B protein of bacteriophage mu is an ATPase that preferentially stimulates intermolecular DNA strand transfer. *Proc Natl Acad Sci USA* 84(3):699–703.
11. Adzuma K, Mizuuchi K (1988) Target immunity of Mu transposition reflects a differential distribution of Mu B protein. *Cell* 53(2):257–266.
12. Miller JL, et al. (1984) The nucleotide sequence of the B gene of bacteriophage Mu. *Nucleic Acids Res* 12(22):8627–8638.
13. Chaconas G, Gloor G, Miller JL (1985) Amplification and purification of the bacteriophage Mu encoded B transposition protein. *J Biol Chem* 260(5):2662–2669.
14. Adzuma K, Mizuuchi K (1991) Steady-state kinetic analysis of ATP hydrolysis by the B protein of bacteriophage mu. Involvement of protein oligomerization in the ATPase cycle. *J Biol Chem* 266(10):6159–6167.
15. Greene EC, Mizuuchi K (2002) Dynamics of a protein polymer: The assembly and disassembly pathways of the MuB transposition target complex. *EMBO J* 21(6): 1477–1486.
16. Greene EC, Mizuuchi K (2004) Visualizing the assembly and disassembly mechanisms of the MuB transposition targeting complex. *J Biol Chem* 279(16):16736–16743.
17. Greene EC, Mizuuchi K (2002) Direct observation of single MuB polymers: Evidence for a DNA-dependent conformational change for generating an active target complex. *Mol Cell* 9(5):1079–1089.
18. Greene EC, Mizuuchi K (2002) Target immunity during Mu DNA transposition. Transpososome assembly and DNA looping enhance MuA-mediated disassembly of the MuB target complex. *Mol Cell* 10(6):1367–1378.
19. Baker TA, Mizuuchi M, Mizuuchi K (1991) MuB protein allosterically activates strand transfer by the transposase of phage Mu. *Cell* 65(6):1003–1013.
20. Surette MG, Harkness T, Chaconas G (1991) Stimulation of the Mu A protein-mediated strand cleavage reaction by the Mu B protein, and the requirement of DNA nicking for stable type 1 transpososome formation. In vitro transposition characteristics of mini-Mu plasmids carrying terminal base pair mutations. *J Biol Chem* 266(5): 3118–3124.
21. Han YW, Mizuuchi K (2010) Phage Mu transposition immunity: Protein pattern formation along DNA by a diffusion-ratchet mechanism. *Mol Cell* 39(1):48–58.
22. Manna D, Higgins NP (1999) Phage Mu transposition immunity reflects supercoil domain structure of the chromosome. *Mol Microbiol* 32(3):595–606.
23. Teplow DB, Nakayama C, Leung PC, Harshey RM (1988) Structure-function relationships in the transposition protein B of bacteriophage Mu. *J Biol Chem* 263(22): 10851–10857.
24. Walker JE, Saraste M, Runswick MJ, Gay NJ (1982) Distantly related sequences in the alpha- and beta-subunits of ATP synthase, myosin, kinases and other ATP-requiring enzymes and a common nucleotide binding fold. *EMBO J* 1(8):945–951.
25. Hung LH, Chaconas G, Shaw GS (2000) The solution structure of the C-terminal domain of the Mu B transposition protein. *EMBO J* 19(21):5625–5634.
26. Yamauchi M, Baker TA (1998) An ATP-ADP switch in MuB controls progression of the Mu transposition pathway. *EMBO J* 17(18):5509–5518.
27. Erzberger JP, Berger JM (2006) Evolutionary relationships and structural mechanisms of AAA+ proteins. *Annu Rev Biophys Biomol Struct* 35:93–114.
28. Wendler P, Ciniawsky S, Kock M, Kube S (2012) Structure and function of the AAA+ nucleotide binding pocket. *Biochim Biophys Acta* 1823(1):2–14.
29. Kelley LA, Sternberg MJE (2009) Protein structure prediction on the Web: A case study using the Phyre server. *Nat Protoc* 4(3):363–371.
30. Söding J, Biegert A, Lupas AN (2005) The HHpred interactive server for protein homology detection and structure prediction. *Nucleic Acids Res* 33(Web Server issue): W244–W248.
31. Penefsky HS (1977) Reversible binding of Pi by beef heart mitochondrial adenosine triphosphatase. *J Biol Chem* 252(9):2891–2899.
32. Ramón-Maiques S, Britton HG, Rubio V (2002) Molecular physiology of phosphoryl group transfer from carbamoyl phosphate by a hyperthermophilic enzyme at low temperature. *Biochemistry* 41(12):3916–3924.
33. Egelman EH (2007) The iterative helical real space reconstruction method: Surmounting the problems posed by real polymers. *J Struct Biol* 157(1):83–94.
34. Ishikawa T, Maurizi MR, Steven AC (2004) The N-terminal substrate-binding domain of ClpA unfoldase is highly mobile and extends axially from the distal surface of ClpAP protease. *J Struct Biol* 146(1–2):180–188.
35. Effantin G, Ishikawa T, De Donatis GM, Maurizi MR, Steven AC (2010) Local and global mobility in the ClpA AAA+ chaperone detected by cryo-electron microscopy: Functional connotations. *Structure* 18(5):553–562.
36. Coros CJ, Sekino Y, Baker TA, Chaconas G (2003) Effect of mutations in the C-terminal domain of Mu B on DNA binding and interactions with Mu A transposase. *J Biol Chem* 278(33):31210–31217.
37. Rappas M, Schumacher J, Niwa H, Buck M, Zhang X (2006) Structural basis of the nucleotide driven conformational changes in the AAA+ domain of transcription activator PspF. *J Mol Biol* 357(2):481–492.
38. Ammelburg M, Frickey T, Lupas AN (2006) Classification of AAA+ proteins. *J Struct Biol* 156(1):2–11.
39. Rappas M, et al. (2005) Structural insights into the activity of enhancer-binding proteins. *Science* 307(5717):1972–1975.
40. Chen Z, Yang H, Pavletich NP (2008) Mechanism of homologous recombination from the RecA-ssDNA/dsDNA structures. *Nature* 453(7194):489–494.
41. Duderstadt KE, Chuang K, Berger JM (2011) DNA stretching by bacterial initiators promotes replication origin opening. *Nature* 478(7368):209–213.
42. Bowman GD, O'Donnell M, Kuriyan J (2004) Structural analysis of a eukaryotic sliding DNA clamp-clamp loader complex. *Nature* 429(6993):724–730.
43. Hui MP, et al. (2010) ParA2, a *Vibrio cholerae* chromosome partitioning protein, forms left-handed helical filaments on DNA. *Proc Natl Acad Sci USA* 107(10):4590–4595.
44. Vecchiarelli AG, et al. (2010) ATP control of dynamic P1 ParA-DNA interactions: A key role for the nucleoid in plasmid partition. *Mol Microbiol* 78(1):78–91.
45. Yanagihara K, Mizuuchi K (2002) Mismatch-targeted transposition of Mu: A new strategy to map genetic polymorphism. *Proc Natl Acad Sci USA* 99(17):11317–11321.
46. Montaño SP, Pigli YZ, Rice PA (2012) The μ transpososome structure sheds light on DDE recombinase evolution. *Nature* 491(7424):413–417.
47. Baker TA, Mizuuchi M, Savilahti H, Mizuuchi K (1993) Division of labor among monomers within the Mu transposase tetramer. *Cell* 74(4):723–733.
48. Bradford MM (1976) A rapid and sensitive method for the quantitation of microgram quantities of protein utilizing the principle of protein-dye binding. *Anal Biochem* 72:248–254.
49. Shaikh TR, et al. (2008) SPIDER image processing for single-particle reconstruction of biological macromolecules from electron micrographs. *Nat Protoc* 3(12):1941–1974.
50. Ludtke SJ, Baldwin PR, Chiu W (1999) EMAN: Semiautomated software for high-resolution single-particle reconstructions. *J Struct Biol* 128(1):82–97.
51. Sorzano CO, et al. (2004) XMIPP: A new generation of an open-source image processing package for electron microscopy. *J Struct Biol* 148(2):194–204.
52. Scheres SH, Núñez-Ramírez R, Sorzano CO, Carazo JM, Marabini R (2008) Image processing for electron microscopy single-particle analysis using XMIPP. *Nat Protoc* 3(6):977–990.
53. Heymann JB, Belnap DM (2007) Bsoft: Image processing and molecular modeling for electron microscopy. *J Struct Biol* 157(1):3–18.